A 3D PRINTING FLEXURE PRESSURE SENSOR FOR ROBOT IMPACT SAFETY TESTING

*Hongliang Shi[1], Yongsik Kim[1], Nicholas Dagalakis[1], Xuechao Duan[2]

[1]Engineering Laboratory, National Institute of Standards and Technology, USA, shi.347@osu.edu

[2]Key Laboratory of Electronic Equipment Structure Design, Xidian University, China

Keywords: 3D printing, pressure sensor, robot safety, flexure structure, stiffness analysis, artifact

Abstract

This paper presents a flexure pressure sensor fabricated by means of 3D printing. This sensor combined with a biosimulant artifact from the National Institute of Standards and Technology (NIST) is used to measure the severity of injuries caused in the case of a robot impact with a human. The stiffness matrix is derived for the structure by means of screw theory. A Finite Element (FE) model is constructed to verify the analytical model and obtain the allowable pressure with regard to the yield stress.

1 Introduction

The movement of manufacturing to countries featuring labor with low hourly wages over the last fifteen years has motivated the development of a new generation of industrial robots that can work side-by-side with human workers [1]. This has created a new technology of Human-Collaboration-Robotics (HCR), which combines the intelligence and dexterity of humans with the strength, repeatability, and endurance of industrial robots [2]. Since most robots are powerful moving machines, the safety of workers working around these robots has become a top priority for safety standards development.

We are using biosimulant materials for the fabrication of inexpensive, disposable HCR safety testing artifacts. These testing artifacts will make possible the measurement of forces, pressure and strain when humans and robots come into contact and also the magnitude of injuries caused by robot static and impact pressure. The Dynamic Impact Testing and Calibration Instrument (DITCI) is a simple instrument, with a significant data collection and analysis capability that is used for the testing and calibration of biosimulant human tissue artifacts [3].

Much work has been done in the design of pressure sensors. Additive manufacturing is widely used for rapid fabrication. Sander et al. [4] designed a monolithic capacitive sensor. Someya et al. [5] designed a flexible pressure sensor matrix for the application of artificial skin. Many Micro-electro-mechanical Systems (MEMS) designs are proposed for pressure sensing [6-12]. However, the costs of these pressure sensors are high. The most common 3D fabrication of polymer objects is fused deposition modeling (FDM). Some other 3D fabrication methods like selective laser melting (SLM), selective laser sintering (SLS), fused filament fabrication (FFF) and stereolithography (SLA) could be used for some other materials or for a higher precision. However, the cost is higher than FDM.

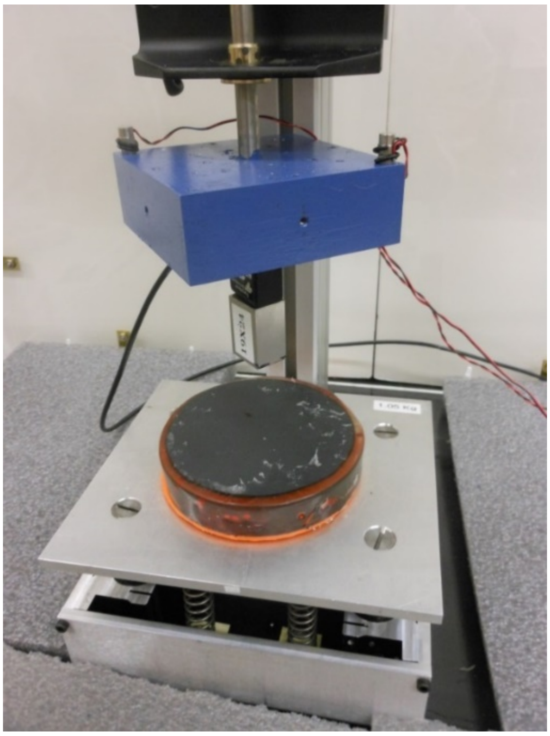

Figure 1. Setting of robot impact testing

In this paper, we propose a structural sensor design, which is mounted underneath the biosimulant artifact. As shown in Fig. 1, the structural sensor mounted under the artifact is set on the DITCI instrument stage. The rest of the paper is organized as follows: Section 2 presents the design methodology and fabrication method. Section 3 derives the stiffness matrices for a single pressure cell. Section 4 presents the finite element analysis (FEA) for the design. Section 5 presents the conclusions.

2 Design and fabrication

In this section, we describe the design and fabrication of the sensor structure. The sensor system includes a top biosimulant artifact and a bottom sensor. We fabricate the sensor by means of FDM.

2.1 Biosimulant artifacts with bottom sensor

As shown in Fig. 2, the sensor system consists of three layers. The top two layers are called the biosimulant artifact, which consists of disks of biosimulant skin and soft tissue [3]. The bottom layer is the structural sensor.

(a) Artifact with pressure sensor

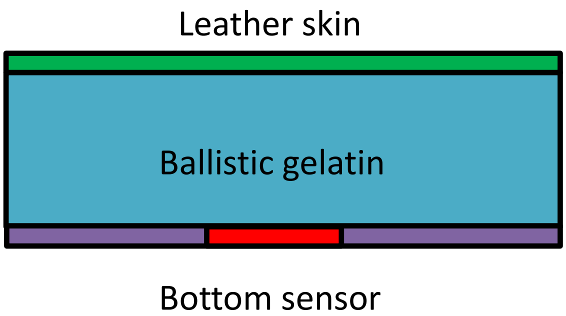

(b) Schematic drawing of artifact with sensor

Figure 2. Biosimulant artifact and bottom sensor

The biosimulant artifact simulates human skin and muscle and simulates the stress distribution when the impact force is applied on the top of the skin. The bottom structural sensor can measure the pressure on the bottom surface of the ballistic gelatin. By studying the distribution of the stress in the ballistic gelatin caused by the dynamic impact force, we build the relationship of the top impact pressure and the pressure distribution on the bottom surface of the ballistic gelatin. Thus, we are able to reconstruct the top impact pressure from the measurements of the calibrated bottom structural pressure sensor.

As shown in Fig. 3, the bottom sensor has two parts: the center structural sensor and a rigid disk. The white structural sensor will be deformed or destroyed at a certain pressure, while the orange rigid plate has no significant deformation during testing. After each impact testing, the white structural sensor is disposed and it can be replaced for multiple testing with the same biosimulant artifact and plate. This setting is designed to reduce disposable material for lower cost. The size of the white structural sensor should be larger than the tool size. Here, we use a 19 mm × 24 mm tool, as show in Fig. 1. The size of the white structural sensor could be changed based on the application.

Figure 3. Bottom plate and pressure sensor

2.2 Design of beam based pressure sensor

The structural sensor is shown in Fig. 4. It mainly consists of three parts: top load cube, middle suspending beam, and bottom holding grid. Each top cube is independently supported by the beam. The two ends of each beam are fixed to the bottom grid. The bottom grid structure is designed to be stiff enough so that no deformation occurs when the loading force impacts on the whole structure. A single pressure cell is composed of one top cube, one beam, and bottom grid. Depending on the contact surface of the tool which is creating the impact force, a certain number of the pressure cells are affected so that the cubes will move downwards. Under sufficient pressure, the supporting beam will be destroyed and the top cube will be driven into the grid structure to show an obvious sign of large deformation.

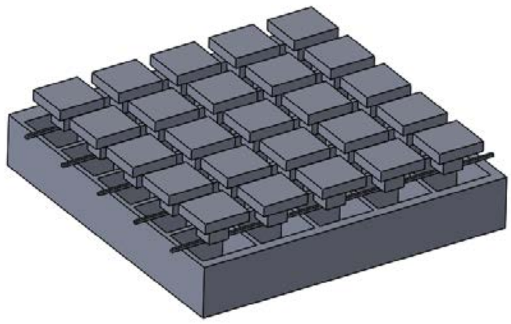

Figure 4. Pressure sensor design

Figure 5 shows a modified design. In this design, the bottom grid has some beams of the grid removed to improve the reliability of the fabrication. Furthermore, the length of each beam is increased to lower the stiffness of the structure. Thus, the allowable pressure can be adjusted. However, the overall size of the sensor is increased.

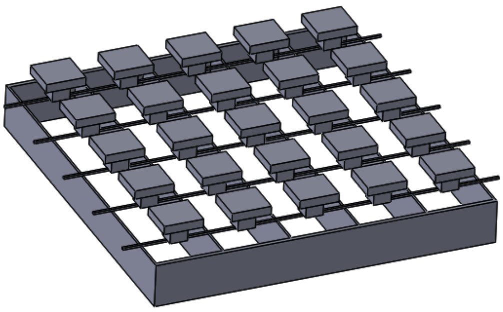

Figure 5. Modified sensor design

2.3 FDM 3D printing fabrication

There are many 3D printers available nowadays. Here, we use a Makerbot Replicator[1] for the fabrication process. As shown in Fig. 6, a single top cubic structure is well printed. The outline is a clear square and there is no extra polymer strings remaining between the squares. We use Makerbot polylactic acid (PLA) as the printing filament material. The printing extrusion and travel speeds are 100 m/s and 45 m/s, respectively. Nozzle temperature is 210 °C and the nozzle size is 0.4 mm in diameter. A well calibrated printer is required to reach the high precision of the printing. Young's modulus of PLA is 3500 N/mm^2 and the yield strength is 45 N/mm^2.

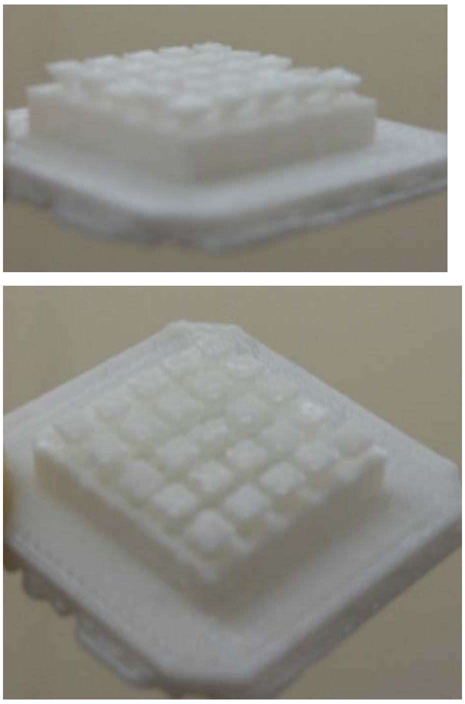

Figure 6. FDM pressure sensor

3 Structural analysis

In this section, the detailed structure of the design is described and later the screw theory based stiffness model is built to calculate the stiffness matrix.

3.1 Design parameters

A schematic drawing of the sensor is shown in Fig. 7. This design is constrained by the capabilities of the 3D printer. With a different type of 3D printing technology, the sensor could be made smaller or from different materials. For example, SLA commonly has a higher resolution and uses cured material like resin.

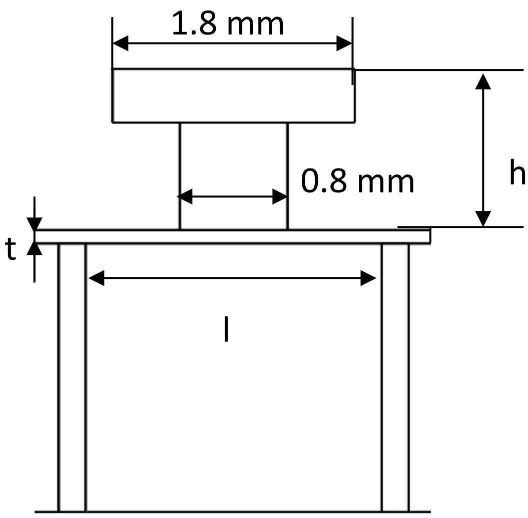

Figure 7. Schematic drawing of sensor

[1] Certain commercial equipment, instruments, or materials are identified in this paper in order to specify the experimental procedure adequately. Such identification is not intended to imply recommendation or endorsement by the National Institute of Standards and Technology, nor is it intended to imply that the materials or equipment identified are necessarily the best available for the purpose.

Here, the suspended beam has a rectangular cross section of thickness t and width w. In order to ensure the printing quality, the value of the supporting beams distance l is set as 2.2 mm. A larger l will cause the printed beam to sag, while a smaller l will cause the gap between the top cubes to be too small. Thus, the remaining polymer strings would reduce the quality. The height h is 1.2 mm.

The top cube also has a minimum printable size. If the size is too small, the top could not maintain the square shape. The ideal design is shown in Fig. 7. However, due to the limitation of FDM 3D printing, the actual shape of the printed sensor is shown in Fig. 8. Careful examination of the printed artifact shows that the end of the attachment to the beam center is reduced to a small square. This is because during FDM printing, the filament could not be fully attached to the beam. We take advantage of this phenomenon to create a better design. This design concentrates the applied force on the beam center to increase the free length of the suspending beam. Finally, the beam is easier to deform with the concentrated force loading on its center. Another feature that needs to be assured in the printing is that the two ends of the beam must be fixed on the bottom grid. As is shown in Fig. 8, the two ends of the beam in the actual design extend over the border so that the nozzle will start at the printing position outside the grid.

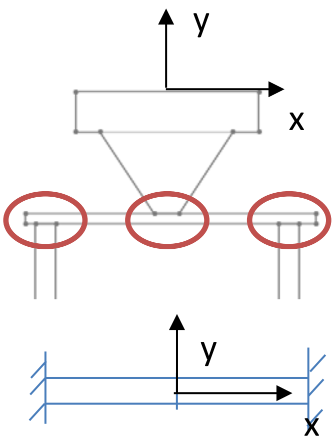

Figure 8. Schematic drawing of FDM sensor

3.2 Stiffness analysis

Here, we adopt the screw theory [13-15] in the analysis of the stiffness matrix. In screw theory, the deformation is denoted by a general twist vector $T = (\theta_x, \theta_y, \theta_z, \delta_x, \delta_y, \delta_z)$ and the loading is denoted by a wrench vector $W = (F_x, F_y, F_z, M_x, M_y, M_z)$. The stiffness matrix is defined *as* $W = [K]T$. Here, the units of the rotational and translational displacement are radian and millimeter, respectively. The units of force and moment are Newton and Newton-millimeter, respectively.

In the stiffness modeling of the sensor structure, we split the beam to two segments from the center plane of the beam. The two segments are considered to be connected in parallel [16-17]. The stiffness of a single beam with rectangular cross section is

$$[K_b] = \frac{EI_z}{l}\begin{bmatrix} 0 & 0 & 0 & \frac{12}{l^2\eta} & 0 & 0 \\ 0 & 0 & -\frac{6}{l} & 0 & \frac{12}{l^2} & 0 \\ 0 & \frac{6}{l\kappa} & 0 & 0 & 0 & \frac{12}{l^2\kappa} \\ \chi\beta & 0 & 0 & 0 & 0 & 0 \\ 0 & \frac{4}{\kappa} & 0 & 0 & 0 & \frac{6}{l\kappa} \\ 0 & 0 & 4 & 0 & -\frac{6}{l} & 0 \end{bmatrix}, \quad (1)$$

where $\eta = t^2/l^2$, $\kappa = I_z/I_y = t^2/w^2, \chi = 1/2(1+\upsilon)$, υ is the Poisson's ratio 0.3 and β is derived from

$$\beta = 12\left(\frac{1}{3} - 0.21\frac{t}{w}\left(1 - \frac{1}{12}\left(\frac{t}{w}\right)^4\right)\right). \quad (2)$$

Through an adjoint transformation matrix $[Ad]$, we could derive the stiffness of the mechanism by means of the equation

$$[K] = [Ad_1][K_w][Ad_1]^{-1} + [Ad_2][K_w][Ad_2]^{-1} \quad (3)$$

where $[Ad_1]$ and $[Ad_2]$ are defined by

$$[Ad] = \begin{bmatrix} R & 0 \\ DR & R \end{bmatrix} \quad (4)$$

Here, $[D]$ is the skew-symmetric matrix defined by the translational vector d [12-13].

$$[R_1] = [X(0)]\ d_1 = (0, h, 0). \quad (5)$$

$$[R_2] = [Z(\pi)]\ d_2 = (0, h, 0). \quad (6)$$

The subscript 1 means left half segment beam and 2 means right half segment beam. After substituting for the material property of PLA, we could obtain the stiffness matrix as

$$[K]=\begin{bmatrix} 0 & 0 & -76.36 & 63.63 & 0 & 0 \\ 0 & 0 & 0 & 0 & 0.52 & 0 \\ 0.63 & 0 & 0 & 0 & 0 & 0.52 \\ 0.79 & 0 & 0 & 0 & 0 & 0.63 \\ 0 & 0.21 & 0 & 0 & 0 & 0 \\ 0 & 0 & 91.85 & -76.36 & 0 & 0 \end{bmatrix} \quad (7)$$

The value 0.52 N/mm is the required force in the y direction for a 1 mm translational displacement.

4 Verification via finite element analysis

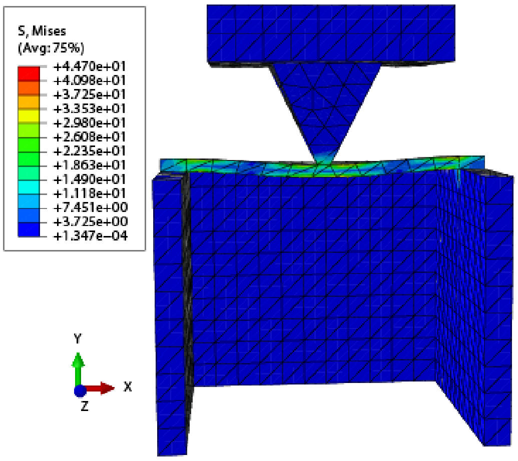

Figure 9. The FE model of a single pressure cell

In order to verify the derivation of the stiffness matrix, we conduct the finite element analysis for the single pressure cell. As shown in Fig. 9, we build the FE model in Abaqus with 4502 elements. The structure is fixed at the bottom and pressure is applied on the top surface. When the maximum Von Mises stress reaches the yield stress of 45 N/mm^2, we record the corresponding loading force and displacement. The top cube moved 0.056 mm downwards with a loading force 0.028 N. The loading force is evenly distributed on the top surface to form the pressure loading.

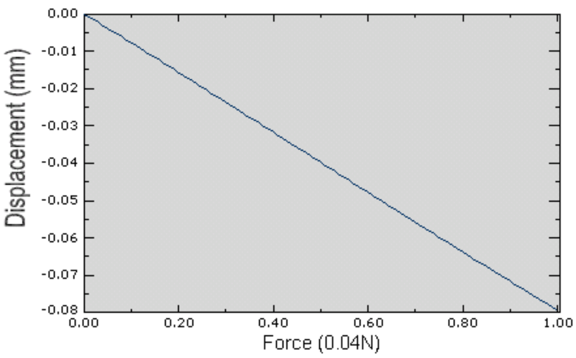

Figure 10. Force vs displacement in the y direction

According to the coordinate frame of Fig. 9, we present the relationship of the force and the displacement in the y direction. As shown in Fig. 10, the beam deforms linearly with respect to the loading. After fitting the points by means of the least squares method, we obtain the value of the stiffness 0.5 N/mm, which is close to the values derived from the stiffness matrix in Eq. 7.

5 Conclusions

This paper presents a structural pressure sensor design fabricated by means of 3D printing. Some meaningful conclusions can be drawn as following.

(1) The structural pressure sensor is disposable, low cost, and easy to fabricate.

(2) We derived the stiffness matrix for a single pressure cell by means of screw theory.

(3) From the result of the FE model, we obtain the loading force 0.028 N. By changing the area of the top surface, we could control the allowable failure pressure.

Acknowledgment

This work was supported by the Robotic Systems for Smart Manufacturing Program of the Intelligent Systems Division, Engineering Laboratory, National Institute of Standards and Technology, USA.

References

[1] Guizzo, E., and Ackerman, E., “How Rethink Robotics Built Its New Baxter Robot Worker,” IEEE Spectrum, 2012,

[2] Pine, A., “Just Ahead: The Robotics Revolution,” Kiplinger Magazine, Jan. 8, 2013

[3] Dagalakis, N.G., Yoo, J.M., and Oeste, T., “Human-Robot Collaboration Dynamic Impact Testing and Calibration Instrument for Disposable Robot Safety Artifacts”, under review.

[4] Sander, C.S., Knutti, J. W., and Meindl, J., “A Monolithic Capacitive Pressure Sensor with Pulse-Period Output”, IEEE Transactions on Electron Device, 1980, 27, (5).

[5] Someya, T., Sekitani, T., Iba, S., Kato, Y., Kawaguchi, H., and Sakurai, T., “A large-area, flexible pressure sensor matrix with organic field-effect transistors for artificial skin applications,” PNAS, 2004, 101, (27), pp. 9966-9970.

[6] Shi, H., Duan, X. C., and Su, H-J. “Workspace optimization of a MEMS hexapod nanopositioner using an adaptive genetic algorithm,” 2014 IEEE International Conference on Robotics and

Automation, (ICRA2014), Hong Kong, May 31-June 7, 2014, pp4043-4

[7] Shi, H., Su, H.-J., and N. Dagalakis, “A stiffness model for control and analysis of a MEMS hexapod nanopositioner”, Mechanism and Machine Theory, 2014, 80, pp. 246-264.

[8] Shi, H., Su, H.-J., Dagalakis, N., and Kramar, J. A., “Kinematic modeling and calibration of a flexure based hexapod nanopositioner,” Precision Engineering, 2013, 37, (1), pp. 117 – 128.

[9] Abeysinghe, D. C., Dasgupta, S., Boyd, J. T., and Jackson, H. E., “A Novel MEMS Pressure Sensor Fabricated on an Optical Fiber”, IEEE Photonics Technology Letters, 2001, 13, (9).

[10] Palasagaram, J. N. and Ramadoss, R., “MEMS - Capacitive Pressure Sensor Fabricated Using Printed-Circuit-Processing Techniques”, IEEE Sensors Journal, 2006, 6, (6).

[11] Krondorfer, R. H., and Kim, Y. K., “Packaging Effect on MEMS Pressure Sensor Performance”, IEEE Transactions on Components and Packaging Technologies, 2007, 30, (2).

[12] Nakamura, K., Iwasaki T. Yamakawa T., and Onishi K., “MEMS pressure sensor”, US Patent, no. 8516905 B2.

[13] Su, H.-J., Shi, H., and Yu, J. “A symbolic formulation for analytical compliance analysis and synthesis of flexure mechanisms,” ASME Journal of Mechanical Design, 2012, 134, (5), pp. 051009-1-9

[14] Shi, H., “Modeling and analysis of compliant mechanisms for designing nanopositioners,” Ph.D. dissertation, OSU, Columbus, MD, 2013.

[15] Su, H.-J., Shi, H., and Yu, J., “Analytical compliance analysis and synthesis of flexure mechanisms,” in Proceedings of ASME IDETC/CIE, Washington, DC, August 28-31, 2011.

[16] Shi, H. and Su, H.-J., “An analytical model for calculating the workspace of a flexure hexapod nanopositioner,” ASME Journal of Mechanisms and Robotics, 2013, 5, (4), p. 041009.

[17] Shi, H. and Su, H.-J., “Workspace of a flexure hexapod nanopositioner,” in Proceedings of ASME IDETC/CIE, 2012, Chicago, Illinois, August 12-15.